Investigations of structures in the parameter space of three-dimensional Turing-like patterns

Martin Skrodzki, Ulrich Reitebuch, Eric Zimmermann

Investigations of structures in the parameter space of three-dimensional Turing-like patterns*

Martin Skrodzki†, Computer Graphics and Visualization, TU Delft
mail@ms-math-computer.science

Ulrich Reitebuch, Institute of Mathematics, FU Berlin
ulrich.reitebuch@fu-berlin.de

Eric Zimmermann, Institute of Mathematics, FU Berlin
eric.zimmermann@fu-berlin.de

Abstract

In this paper, we are interested in classifying the different arising (topological) structures of three-dimensional Turing-like patterns. By providing examples for the different structures, we confirm a conjecture regarding these structures within the setup of three-dimensional Turing-like pattern. Furthermore, we investigate how these structures are distributed in the parameter space of the discrete model. We found two-fold versions of so-called "zero-" and "one-dimensional" structures as well as "two-dimensional" structures and use our experimental findings to formulate several conjectures for three-dimensional Turing-like patterns and higher-dimensional cases.

*This material is based upon work supported by the National Science Foundation under Grant No. DMS-1439786 and the Alfred P. Sloan Foundation award G-2019-11406 while the author was in residence at the Institute for Computational and Experimental Research in Mathematics in Providence, RI, during the Illustrating Mathematics program; This research was partially funded by the Deutsche Forschungsgemeinschaft (DFG, German Research Foundation) – 455095046; Furthermore, this research was supported by the DFG Collaborative Research Center TRR 109, "Discretization in Geometry and Dynamics", RIKEN iTHEMS, and the German National Academic Foundation.

†corresponding author

1 Introduction

In his 1952 paper "The chemical basis of morphogenesis", Alan M. Turing presented a model for the formation of skin patterns [10]. While it took several decades, the model has been validated by finding corresponding natural phenomena, e.g., in the skin pattern formation of zebrafish [1, 7]. More surprising, seemingly unrelated pattern formations can also be studied via the model, like e.g., the formation of plant patches around termite hills [6]. Furthermore, three-dimensional Turing patterns have been observed in microemulsions [2] as well as in physical simulations [3].

In 1984, David A. Young proposed a discretization of Turing's model, reducing it to an activator/inhibitor process on a discrete domain [12]. This model can be easily extended to the concept of three-dimensional Turing-like patterns [8]. While the parameter space for two-dimensional Turing patterns has been investigated in the context of predator-prey models [11] or Ising models [5], no such investigation is available for the three-dimensional Turing-like patterns resulting from the extension of Young's cellular automaton. This exploratory paper presents several findings and conjectures on the parameter space of these automata.

2 Three-dimensional Turing-like pattern from CA

Based on previous models for patterns in the visual cortex of the brain ([9]), Young presented his own two-morphogen model, see [12]. He assumes two types of cells: differentiated (pigmented) cells (DCs) and undifferentiated cells (UCs). Then, each DC produces an activator morphogen M^1 which differentiates nearby UCs and an inhibitor morphogen M^2 which causes nearby DCs to become undifferentiated. From this model, Turing-like patterns are obtained by starting with a rectangular grid of cells. We will model a cell at position (x, y) in the grid by its *state* $s_t(x, y) \in \{0, 1\}$ at time t, indicating a DC ($s_t(x, y) = 1$) or UC ($s_t(x, y) = 0$).

Initially, each cell is chosen to be a DC according to some random process. To determine the state of a cell (x, y) in the next time step, compute

$$s_{t+1}(x, y) = \begin{cases} 1 & \tilde{\sum} > 0, \\ s_t(x, y) & \tilde{\sum} = 0, \\ 0 & \tilde{\sum} < 0, \end{cases} , \tag{1}$$

with $\tilde{\sum} = \sum_{(x',y') \in B_{R_2}(x,y)} \omega_{t,(x,y)}(x', y')$, where $B_{R_2}(x, y)$ is the ball of radius R_2 around (x, y) and

$$\omega_{t,(x,y)}(x', y') = \begin{cases} 0 & (x - x')^2 + (y - y')^2 > R_2^2, \\ w_1 \cdot s_t(x', y') & (x - x')^2 + (y - y')^2 < R_1^2, \\ w_2 \cdot s_t(x', y') & \text{otherwise.} \end{cases} \tag{2}$$

That is, for any grid cell (x, y), all DCs within the circular region of radius R_2 are taken into account. Those that lie within the smaller circular region of radius R_1 contribute weight w_1 while those in the annulus between R_1 and R_2 contribute weight w_2. If the sum of these weights is positive, the cell becomes differentiated; if the sum is zero, the cell does not change its state; if the sum is negative, the cell becomes undifferentiated. Note that the domain is assumed to be toroidal, i.e., two opposite borders are identified with each other.

In order to lift this model to a three-dimensional domain, the single necessary addition is a term $(z - z')^2$ in the right-hand side of Equation (2). To further simplify Young's approach, it can be reduced to choosing initial DCs in the domain uniformly randomly with some probability $\rho \in [0, 1]$ and furthermore fixing $w_1 = 1$, $w_2 = -1$, see [8]. Given a domain size, these simplifications reduce the parameter space of Turing-like patterns to choosing a probability $\rho \in [0, 1]$ as well as two radii R_1 and R_2. It is this three-dimensional parameter space that we aim to investigate in the following.

3 Fixing a finite parameter space

In order to experimentally investigate the parameter space spanned by R_1, R_2, and ρ, we first fix the size of the cubical three-torus to work on. To be able to fully classify the entire parameter space, we chose a grid size of $70 \times 70 \times 70$. Choosing too large values for the radii R_1 and R_2 in a comparably small domain would obscure the patterns formed. Therefore, we reduced the choice for the two radii to be from $\{1, \ldots, 40\} \subset \mathbb{N}$. The value ρ determines the probability of initial activity of each cell in our cubical grid. To discretize the probability, we chose a domain $\mathcal{I} := \{0, \ldots, n_\rho\} \subset \mathbb{N}$ with $n_\rho = 120$. As the probabilities $\rho = 0$ and $\rho = 1$ only provide completely undifferentiated or completely differentiated[1] domains respectively, we chose the lowest probability to be investigated to be at $\exp(-\min_\rho)$ with $\min_\rho = 12$, i.e., the lowest probability as $\exp(-12) \approx 6 \cdot 10^{-6}$. As [8] found their zero-dimensional behavior for extremely large values of ρ, we decided to discretize this dimension of the parameter space non-linearly. Therefore, the domain is mapped to a probability value via the following sigmoid

$$\begin{aligned} \sigma : \mathcal{I} &\to [0, 1], \\ x &\mapsto \frac{\exp\left(2 \cdot \min_\rho \cdot n_\rho^{-1} \cdot x - \min_\rho\right)}{1 + \exp\left(2 \cdot \min_\rho \cdot n_\rho^{-1} \cdot x - \min_\rho\right)}, \end{aligned} \tag{3}$$

which provides good resolutions at very low and very high probabilities as well as a decent resolution of the behavior between these extremes. In the following, we will assume that some $x \in \mathcal{I}$ was chosen and simply write $\rho := \sigma(x)$ for brevity.

[1] Note that complete DCs can turn to complete UCs within one step, e.g., if $R_2 \gg R_1$.

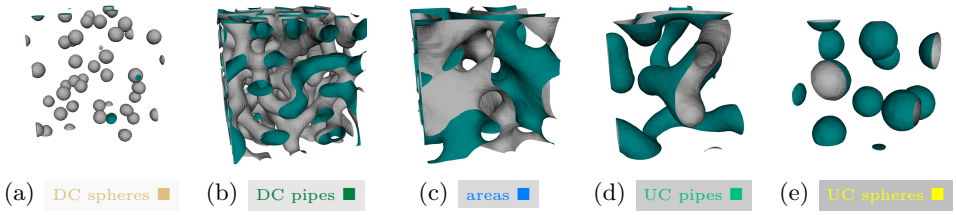

Figure 1: Five of the seven possible Turing-like patterns in a three-torus, with the trivial cases of all DCs or all UCs not shown. The images show the isosurface separating DC (green) and UC (gray) cells. Patterns include sphere-like structures, (a) and (e), pipe-like structures, (b) and (d), and area-spanning structures (c)).

The three parameters ρ, R_1, and R_2 span a $121 \times 40 \times 40$ grid where each included triple gives rise to a Turing-like pattern. Considering the types of structures found in previous work [3, 2, 8], we expect to find seven different types of structures that can form in the three-dimensional domain. Two of these are the trivial patterns of only differentiated or only undifferentiated cells. The remaining five structures are displayed in Figure 1. Note that for the visualization of three-dimensional patterns, a different approach is necessary than for two-dimensional patterns, in order to gain insights into the presented structures. Thus, following [8], the renderings in Figure 1 show only the isosurface between regions of DCs (green) and UCs (gray). Shrinking the structures by a factor of approximately R_1, we reduce them as follows: spheres become 0-dimensional points, tubes become 1-dimensional strands, and areas remain 2-dimensional. In the following, we refer to the patterns by these "dimension" values.

Observe, that except for the 2-dimensional case, we obtain two possible scenarios for 0-dimensional and 1-dimensional structures, which come from the distinction into interior and exterior cell types. The following experimental part of the project now consists of partitioning the discretized parameter space into these seven cases, i.e., identifying for each parameter triple (ρ, R_1, R_2) which type of Turing-like pattern arises.

4 Exploration of the parameter space

Our exploration of the parameter space consisted of picking a parameter triple and starting the CA of [8] with it. After the automaton had either converged or after 20 iterations/seconds had passed, the current state was rendered using the *Marching Cubes Algorithm* [4]. The experimentalist then classified the visualized pattern according to their closest resemblance with the images in Figure 1 or (if the pattern clearly had not converged yet) continued the generation for several more iterations.

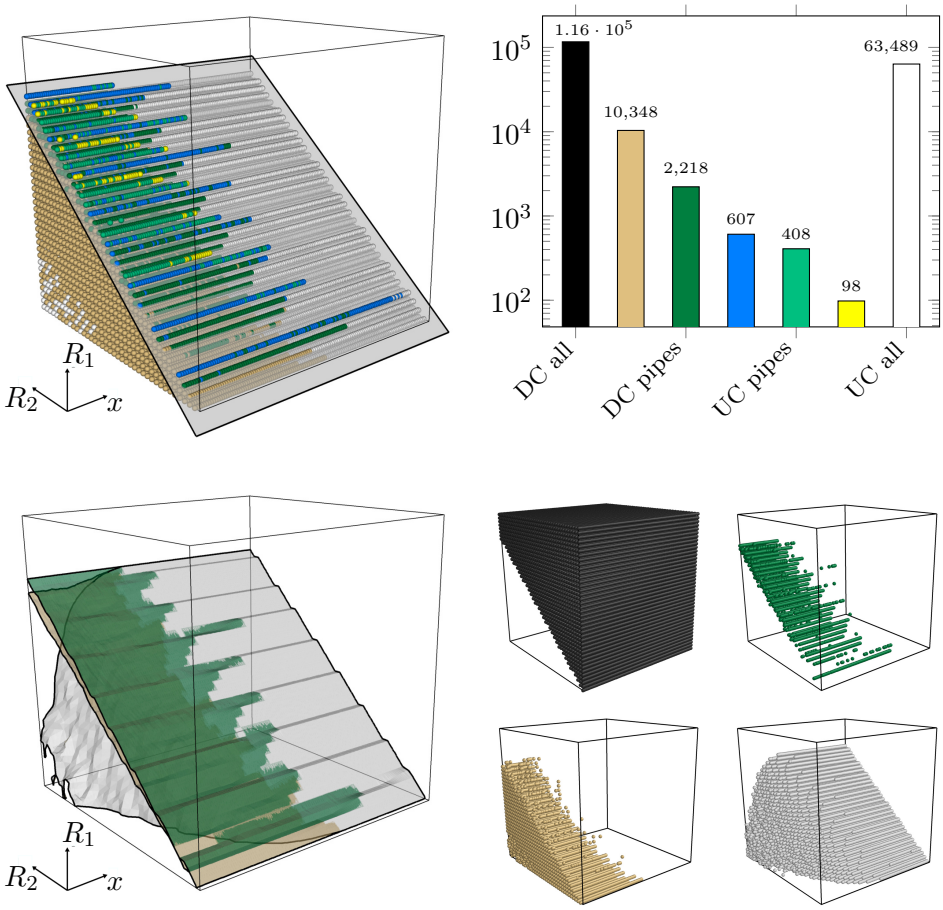

Figure 2: **Top and bottom left**: Plot of the three-dimensional parameter space consisting of activator radius R_1, inhibitor radius R_2, and activation (x as argument for $\rho = \sigma(x)$). The parameter triples are colored by found structures. In the top left image, the shown hyperplane with increase $\sqrt[3]{2}^{-1}$ indicates equal volume covered by the R_1 ball and the R_2 annulus. Note that the color for all-DC triples is black, and we disabled their rendering for enhanced visibility of the other structures. Note further that the x-axis is not a linear depiction of the activation probability, but the argument for $\sigma(x)$, see Equation (3). **Top right**: Histogram over the found structures. Note that the y-axis in the histogram follows a logarithmic scale. **Bottom left**: Separating isosurfaces of volumetric distributed triples "UC all" (behind white), "DC spheres" (between white and beige), "DC pipes" (between beige and green), and "DC all" (remaining volume on top). **Bottom right**: The respective triple groups from the parameter set, giving rise to the separating isosurfaces. All figures follow the color coding according to Figure 1.

The distribution of structures in our segment of the parameter space is shown in a histogram in Figure 2. The dominating structure is "DC all" followed by "UC all", which enclose all other structures in the parameter space. This encapsulating behavior can be seen in the two-dimensional layers of the parameter space shown in the left images of Figure 2, where the "DC all" states reside on top and the "UC all" states on the opposing side of the parameter cube. Note that in the left of Figure 2 and in the upcoming illustrations, we decided to neglect the "DC all" triples for visual reasons: Rendering these would hide the distribution of the other structures within the parameter space. Going back to the histogram in Figure 2, the remaining non-trivial structures follow with decreasing amount, with "UC pipes" and "UC spheres" having the rarest occurrences.

One first trivial observation regarding the distribution of structures can be drawn from the behavior of the activator and inhibitor radii: If $R_1 \geq R_2$, all cells are differentiated (given that the random process guided by $\rho > 0$ creates at least one active cell), because the inhibitor range does not have any impact.

When considering the special case of the volume of the activator ball and the inhibitor annulus around it being equal, we obtain:

$$\frac{4}{3}\pi R_1^3 = \frac{4}{3}\pi R_2^3 - \frac{4}{3}\pi R_1^3 \quad \Rightarrow \quad R_1 = \frac{R_2}{\sqrt[3]{2}}.$$

Thus, we can separate the entire three-dimensional parameter space by a separating hyperplane, see Figure 2, top left. Above this separation, the triples are more likely to produce "DC all" structures and below it, they tend to form "UC all" structures. However, as we are dealing with a discretization—i.e., the volume of kernels is not $\frac{4}{3}\pi R_i^3$, $i = 1, 2$ but the number of discrete cells within—the obtained structures in our experiments deviate from this theoretical assertion. All such structures ("areas", "UC pipes", and "spheres") occur in the vicinity of this linear separation, see Figure 2, top left.

Within our discretization of the parameter space, we find that those triples form volumetric groups that give rise to the following four structures: "UC all", "DC all", "DC pipes", and "DC spheres". On the lower left of Figure 2, we draw isosurfaces in white, beige, and dark green that separate the respective triple groups, which are shown in the bottom right. From the dark green up to the beige isosurface, we find a slender wedge consisting of "DC pipes". The volume between the beige isosurface and the highly non-planar white surface is filled with "DC spheres" while the rest of the parameter space consists of "UC all". The other structures ("areas", "UC pipes", and "UC spheres") do not obtain volumetric extent in our discretization and with the chosen parameter bounds. They all lie close to the linear separation plane shown in the top left of Figure 2. These observations motivate two conjectures.

Conjecture 1 *The wedge, formed in the parameter space by the "DC pipes" triples, given as volume between the beige and dark green isosurface, Figure 2, will grow larger and wider with increasing values for R_1 and R_2.*

Conjecture 2 *The collections of parameter triplets associated to the structures: "areas", "UC pipes", and "UC spheres" will gain volumetric extent in the parameter space when increasing the maximal values of R_1 and R_2.*

From the above discussion, it is clear that we were able to find all structures displayed in Figure 1. Thereby, we positively answer a corresponding conjecture, posed in [8]. Our experiments lead us to the following conjecture.

Conjecture 3 *A Turing-like pattern of dimension d (cf. 1) exhibits structures of all dimensions from 0 to $d-1$. Furthermore, each structure of dimension $0, \ldots, d-2$ occurs twice as "UC" and "DC" version, while structures of dimension $d-1$ appear only once.*

5 Towards automatic structure classification

The classification in our experiments where visually guided and depended to a certain extent on the experimentalist. This section is devoted to investigating an automatic classification of the found structures, based on the obtained data. Two entities of interest are the volume and surface area of the structures. The scatterplots shown in Figure 3 suggest that the structures are characterized to a large extend by their volume. Indeed, a corresponding histogram and a violin plot of the volume distribution confirm this first suspicion, see Figure 4.

Based on these preliminary analyses, we aim at building a predictor for the structure type, based on the volume found. We use a total of $2,214$ hand-classified structures to train the predictor. Note that this data is not uniformly selected, but rather chosen along the border of larger patches as shown in Figure 2. For cross-correlation, we separate the data set into five folds, with the distribution of structures as shown in Table 1. To train our

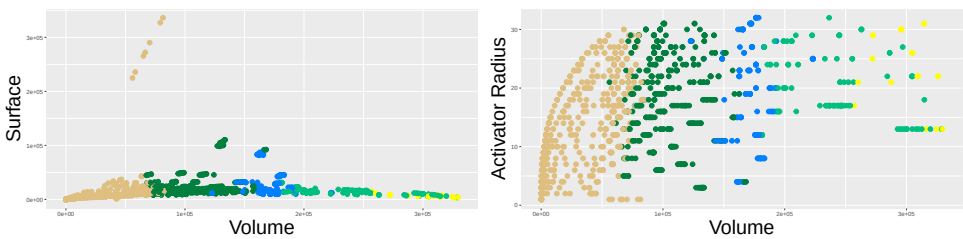

Figure 3: Two plots indicating the relation between volume and surface area (left) as well as volume and activator radius (right) of the structures.

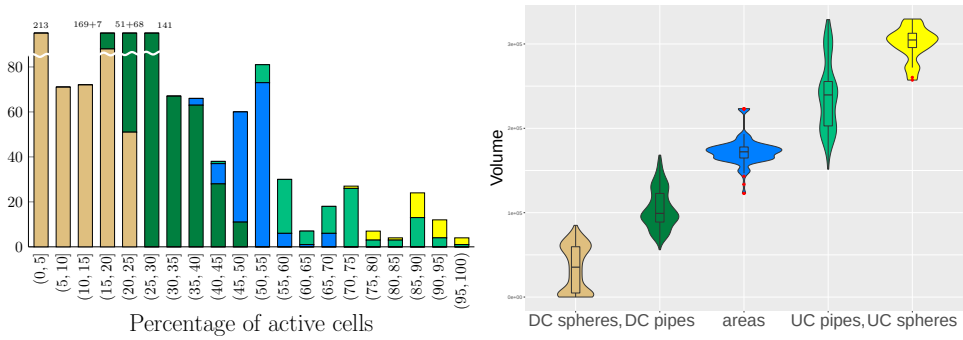

Figure 4: **Left:** Histogram over 2,214 data points from the parameter space, selected from the border of two structure areas. The bins on the x-axis represent the percentage of activated cells in the final state (excluding "UC all" and "DC all" at the far ends). The stacked bars are colored following the color scheme of Figure 1. Bars are printed up to 85 elements and cut from there, where the actual values are given on top. **Right:** Violin plot over the different types of structures, indicating the distribution of the volume that is taken by each structure. Note the box-plot overlay indicating the mean as well as the first and third quartile. Outliers are shown in red, most notably for the "areas". Furthermore, "UC pipes" and "UC spheres" do not show a clear separation by their volume.

predictor, we perform the following operation on all folds. For two neighboring structure types, we use the training data (all data points not in the fold) to find a certain volume-threshold to optimally distinguish these. Thus, we obtain four volume-thresholds for each fold, indicating five intervals that are associated with the respective structures. Then, we use these thresholds to classify the testing data from the fold, where we report an error if the hand-classified label does not agree with the threshold label of the structure, see Table 1. Overall, the prediction of the structure by the volume admits an average classification error of 8.39%. While this indicates the volume to be a very strong predictor, the results differ drastically over the different structures. While "DC spheres" exhibit an extremely low classification error of 3.47% across all folds and "DC pipes" are within the average with an error of 8.05%, all other three structures have way larger classification error, with 42.86% of "UC spheres" being wrongly classified, see Table 1. This confirms the impression from Figure 4 that "UC pipes" and "UC spheres" are not well separated solely by their volume.

The scatterplots in Figure 3 suggest that the surface area of the structure does not carry a lot of information regarding the type of the structure, but that the activator radius, in conjunction with the volume, could provide a better classifier. On the same folds as used above, we train a k-nearest neighbor predictor. The used neighborhood sizes were $k \in \{1, \ldots, 20\}$. As

	Fold1	Fold2	Fold3	Fold4	Fold5	Error (%)
"DC spheres"	116	115	115	115	115	3.47
"DC pipes"	77	77	77	77	77	8.05
"areas"	29	30	29	30	29	14.97
"UC pipes"	20	20	20	20	21	18.81
"UC spheres"	6	6	5	6	5	42.86
Error (%)	7.26	9.27	8.06	9.68	7.66	

Table 1: Distribution of the different structures over the folds of the data set used for cross-correlation. The errors given indicate classification errors of the structures solely based on the volume of the structure.

the two features, volume and activator radius, exhibit very different sizes, we normalize these two dimensions to exclude any artifacts. For our data set and the number of chosen folds, we obtain a minimal classification error for $k = 1$, where the mean classification error over all folds is 7.35%. Thus, most of the information on structures is already captured by the volume and the activator radius only provides a minimal gain in information.

Considering that the data is randomly generated and hand-classified, the predictors presented here already obtain a high level of accuracy. It is clear from our findings that the volume of a structure is the best predictor for its type. Further research is necessary to provide more precise classifications.

6 Conclusion

In this paper, we have presented a visually-guided investigation of structures in three-dimensional Turing-like patterns. Based on a discretization, we gave a complete partition of a finite portion of the parameter space and found five different non-trivial structures, see Figure 1. Thereby, we confirmed a conjecture of [8], who proposed the existence of two-dimensional structures in three-dimensional Turing-like patterns. Based on our experiments, we furthermore provided statistical insight into the distribution of the different structures within the parameter space. From these data, we presented several conjectures both regarding three- and higher-dimensional Turing-like patterns.

Future research has to be directed at finding a thorough mathematical description of the different structures described in this work, e.g., based on the number of connected components or the Euler characteristic. We have shown that the volume is a strong predictor to classify the "DC" structures, but it does not work well on the "UC" structures. Furthermore, a larger portion of the parameter space has to be investigated to better understand the zero-, one-, and two-dimensional structures that arise. The experiments presented in this paper can help narrow down a corresponding portion of the parameter space and thus help focus on the relevant parts.

References

[1] Rihito Asai, Emiko Taguchi, Yukari Kume, Mayumi Saito, and Shigeru Kondo. Zebrafish leopard gene as a component of the putative reaction-diffusion system. *Mechanisms of development*, 89(1-2):87–92, 1999.

[2] Tamás Bánsági, Vladimir K. Vanag, and Irving R. Epstein. Tomography of reaction-diffusion microemulsions reveals three-dimensional turing patterns. *Science*, 331(6022):1309–1312, 2011.

[3] Teemu Leppänen, Mikko Karttunen, Kimmo Kaski, Rafael A Barrio, and Limei Zhang. A new dimension to turing patterns. *Physica D: Nonlinear Phenomena*, 168:35–44, 2002.

[4] William E. Lorensen and Harvey E. Cline. Marching cubes: A high resolution 3d surface construction algorithm. *ACM siggraph computer graphics*, 21(4):163–169, 1987.

[5] Mélody Merle, Laura Messio, and Julien Mozziconacci. Turing-like patterns in an asymmetric dynamic ising model. *Physical Review E*, 100(4):042111, 2019.

[6] Robert M. Pringle and Corina E. Tarnita. Spatial self-organization of ecosystems: integrating multiple mechanisms of regular-pattern formation. *Annual review of Entomology*, 62:359–377, 2017.

[7] Jake Cornwall Scoones and Tom W. Hiscock. A dot-stripe turing model of joint patterning in the tetrapod limb. *Development*, 147(8), 2020.

[8] Martin Skrodzki and Konrad Polthier. Turing-like patterns revisited: A peek into the third dimension. In *Proceedings of Bridges 2017: Mathematics, Art, Music, Architecture, Education, Culture*, pages 415–418. Tessellations Publishing, 2017. Available online at http://archive.bridgesmathart.org/2017/bridges2017-415.pdf.

[9] Nicolas V Swindale. A model for the formation of ocular dominance stripes. *Proceedings of the Royal Society of London. Series B. Biological Sciences*, 208:243–264, 1980.

[10] Alan Mathison Turing. The chemical basis of morphogenesis. *Philosophical Transactions of the Royal Society of London. Series B, Biological Sciences*, 237(641):37–72, 1952.

[11] Vagner Weide Rodrigues, Diomar Cristina Mistro, and Luiz Alberto Díaz Rodrigues. Pattern formation and bistability in a generalist predator-prey model. *Mathematics*, 8(1):20, 2020.

[12] David A. Young. A local activator-inhibitor model of vertebrate skin patterns. *Mathematical Biosciences*, 72(1):51–58, 1984.